The Astrophysical Journal, 771:39 (12pp), 2013 July 1 doi:10.1088/0004-637X/771/1/39

THE 300 km s^{-1} STELLAR STREAM NEAR SEGUE 1: INSIGHTS FROM HIGH-RESOLUTION SPECTROSCOPY OF ITS BRIGHTEST STAR*

Anna Frebel[1], Ragnhild Lunnan[2], Andrew R. Casey[1,3], John E. Norris[3], Rosemary F. G. Wyse[4], and Gerard Gilmore[5]
[1] Massachusetts Institute of Technology, Kavli Institute for Astrophysics and Space Research, 77 Massachusetts Avenue, Cambridge, MA 02139, USA
[2] Harvard-Smithsonian Center for Astrophysics, 60 Garden Street, Cambridge, MA 02138, USA
[3] Research School of Astronomy & Astrophysics, The Australian National University, Mount Stromlo Observatory, Cotter Road, Weston, ACT 2611, Australia
[4] Department of Physics & Astronomy, The Johns Hopkins University, 300 N. Charles Street, Baltimore, MD 21218, USA
[5] Institute of Astronomy, University of Cambridge, Madingley Road, Cambridge CB3 0HA, UK
Received 2012 December 5; accepted 2013 April 29; published 2013 June 13

ABSTRACT

We present a chemical abundance analysis of 300S-1, the brightest likely member star of the 300 km s^{-1} stream near the faint satellite galaxy Segue 1. From a high-resolution Magellan/MIKE spectrum, we determine a metallicity of [Fe/H] $= -1.46 \pm 0.05 \pm 0.23$ (random and systematic uncertainties) for star 300S-1, and find an abundance pattern similar to typical halo stars at this metallicity. Comparing our stellar parameters to theoretical isochrones, we estimate a distance of 18 ± 7 kpc. Both the metallicity and distance estimates are in good agreement with what can be inferred from comparing the Sloan Digital Sky Survey photometric data of the stream stars to globular cluster sequences. While several other structures overlap with the stream in this part of the sky, the combination of kinematic, chemical, and distance information makes it unlikely that these stars are associated with either the Segue 1 galaxy, the Sagittarius Stream, or the Orphan Stream. Streams with halo-like abundance signatures, such as the 300 km s^{-1} stream, present another observational piece for understanding the accretion history of the Galactic halo.

Key words: Galaxy: halo – Galaxy: kinematics and dynamics – stars: abundances

Online-only material: color figures

1. INTRODUCTION

In the ΛCDM model, structure builds up hierarchically, with smaller objects merging to build larger ones. One consequence of this is stellar streams in the Galactic halo, produced as accreted objects are tidally disrupted (see, e.g., Lynden-Bell 1995, and references therein). A well-known example is the stream extending from the Sagittarius dwarf spheroidal, which has been traced more than one full wrap around the Milky Way (e.g., Ibata et al. 1994; Majewski et al. 2003). In a part of the sky dubbed the "Field of Streams" (Belokurov et al. 2006), at least two wraps of the Sagittarius Stream as well as several other structures are visible.

A new velocity structure in this field has recently been discovered overlapping with the ultra-faint object Segue 1 (Belokurov et al. 2007b). Radial velocity data to determine Segue 1's velocity dispersion by Geha et al. (2009) revealed a group of stars moving near 300 km s^{-1} (with dispersion of ∼10 km s^{-1}). For comparison, the Segue 1 dwarf has a mean velocity of 208 km s^{-1} with a dispersion of 3 km s^{-1} (Simon et al. 2011, hereafter S11). The same overdensity of stars at this velocity was seen by Norris et al. (2010, hereafter N10), and in the larger spectroscopic sample of Segue 1 stars of S11. The stars have so far been interpreted as part of a stellar stream independent of Segue 1, and we shall refer to it as the "300 km s^{-1} stream" or "300S" throughout this paper. Since the full extent of this structure has not been mapped out, however, it is also possible that these stars belong to a bound object.

From the Sloan Digital Sky Survey (SDSS) photometry, one can obtain an estimate of the distance and metallicity of the 300 km s^{-1} stream by comparing the color–magnitude diagram to globular cluster sequences and isochrones. To further characterize the stream chemically, however, high-resolution spectroscopy is necessary. Here, we present the first high-resolution spectrum and detailed abundance analysis of a star in 300S.

This paper is organized as follows. In Section 2, we briefly discuss the sample from which the main target for high-resolution spectroscopy was selected. The observations and basic spectral analysis of our target star are presented in Section 3, and the abundance analysis in Section 4. We interpret the results in Section 5, and discuss the nature and potential origin of the stream in Section 6.

2. STREAM SAMPLE AND TARGET SELECTION

There are two existing medium-resolution spectroscopic studies of the region around the ultra-faint dwarf galaxy Segue 1, N10 and S11. N10's data were obtained with the Anglo-Australian Telescope's AAOmega spectrograph, which can take simultaneous spectra of 400 targets over a field 2° in diameter. They were targeting stars in the red giant branch (RGB) locus. S11, on the other hand, were using the DEIMOS spectrograph on the Keck II telescope, focusing on an area within ∼15′ of the center of Segue 1, and going deeper than N10. Table 1 lists all stars (52 total) in the two samples with heliocentric radial velocities higher than 240 km s^{-1}. This value corresponds to about the cutoff of Segue 1 dwarf galaxy stars in S11 (their Figure 3). It conservatively includes all stars with velocities that are not consistent with Segue 1 membership, and hence potential 300S candidates. The estimated velocity uncertainty for the N10 stars is 10 km s^{-1}; the individual velocity uncertainties for S11 stars are shown in the table. The list includes four targets from the AAOmega sample not published in N10 due to slightly

* This paper includes data gathered with the 6.5 m Magellan Telescopes located at Las Campanas Observatory, Chile.

Table 1
Stream Member Candidate Stars

Identifier	R.A. (J2000)	Decl. (J2000)	g	r	i	$g-r$	$V_{\rm helio}$ (km s^{-1})	Ref.
300S-1[a]	10 09 15.0	+15 59 48.4	17.99	17.49	17.26	0.73	307	N10
300S-2	10 07 40.1	+16 03 09.7	19.96	19.55	19.44	0.52	298/303.1 ± 3.1	N10/S11
300S-3	10 06 59.0	+15 44 18.8	19.72	19.33	19.14	0.58	307	N10
300S-4	10 06 51.8	+15 49 41.5	20.36	20.04	19.91	0.45	300	AAO
300S-5	10 06 20.0	+15 46 12.7	20.09	19.78	19.67	0.42	315	AAO
300S-6	10 06 12.0	+15 45 48.4	20.08	19.62	19.61	0.47	327	N10
300S-7	10 05 30.6	+15 54 18.1	19.83	19.49	19.31	0.52	305	N10
300S-8	10 06 27.7	+15 54 08.6	20.15	19.88	19.71	0.44	300	AAO
300S-9	10 06 47.7	+16 13 30.1	20.01	19.70	19.51	0.50	300	AAO
300S-10	10 06 58.5	+16 20 45.6	19.84	19.37	19.18	0.66	295	N10
300S-11	10 08 39.7	+16 28 26.7	19.16	18.73	18.60	0.56	288	N10
300S-12	10 06 00.2	+16 05 18.6	20.22	19.68	19.51	0.71	242	N10
300S-13	10 06 18.7	+16 03 39.0	21.67	21.14	20.90	0.77	268.6 ± 3.1	S11
300S-14	10 06 20.0	+16 00 42.1	21.70	21.41	21.18	0.52	305.5 ± 4.3	S11
300S-15	10 06 30.9	+16 15 12.1	21.47	21.13	20.95	0.52	321.0 ± 8.8	S11
300S-16	10 06 42.8	+15 57 09.3	21.56	21.23	21.02	0.54	291.9 ± 6.4	S11
300S-17	10 06 46.8	+16 06 08.3	20.53	20.22	20.07	0.46	294.5 ± 2.9	S11
300S-18	10 06 48.5	+16 09 58.1	20.27	19.98	19.79	0.48	306.0 ± 2.6	S11
300S-19	10 06 50.8	+16 03 51.2	22.13	21.95	21.83	0.30	312.6 ±11.9	G09, S11
300S-20	10 06 54.2	+15 55 20.7	22.12	21.53	21.29	0.83	268.5 ± 6.2	S11
300S-21	10 06 56.1	+16 06 60.0	21.34	21.09	20.99	0.35	302.0 ± 2.6	S11
300S-22	10 06 58.5	+15 57 48.9	21.56	21.09	20.84	0.72	290.5 ± 3.6	S11
300S-23	10 07 04.6	+16 01 30.8	21.22	20.81	20.76	0.46	295.8 ± 3.9	S11
300S-24	10 07 04.6	+16 08 12.6	21.08	20.85	20.74	0.34	296.9 ± 3.4	S11
300S-25	10 07 08.4	+15 56 46.3	22.03	21.56	21.45	0.58	286.3 ± 5.4	S11
300S-26	10 07 09.1	+16 04 36.6	22.29	21.88	21.57	0.72	312.7 ± 6.4	S11
300S-27	10 07 09.7	+15 53 12.3	16.11	15.83	15.72	0.39	303.4 ± 2.2	S11
300S-28	10 07 13.0	+15 57 34.8	18.28	18.00	17.87	0.41	307.9 ± 2.4	S11
300S-29	10 07 13.7	+16 04 44.8	22.13	21.76	21.47	0.66	293.4 ± 4.8	G09, S11
300S-30	10 07 15.5	+16 05 52.1	20.36	20.07	19.97	0.39	282.0 ± 2.8	S11
300S-31	10 07 15.5	+16 15 19.1	20.74	20.43	20.42	0.32	266.8 ± 3.1	S11
300S-32	10 07 17.2	+16 05 11.9	22.10	21.78	21.38	0.72	266.3 ± 4.4	S11
300S-33	10 07 17.4	+16 03 55.6	20.11	19.77	19.64	0.47	295.9 ± 2.4	G09, S11
300S-34	10 07 20.0	+16 01 37.5	17.62	17.27	17.12	0.50	312.7 ± 2.2	S11
300S-35	10 07 21.2	+16 11 18.2	20.99	19.73	19.20	1.79	281.6 ± 2.4	S11
300S-36	10 07 21.8	+15 54 24.5	20.61	20.22	20.22	0.39	307.2 ± 5.5	S11
300S-37	10 07 29.6	+16 11 07.1	20.35	19.34	19.02	1.33	309.6 ± 2.2	S11
300S-38	10 07 32.5	+16 05 00.5	22.58	22.04	21.91	0.67	281.1 ± 6.9	G09, S11
300S-39	10 07 35.0	+15 54 31.5	20.78	20.54	20.39	0.39	303.2 ± 2.8	S11
300S-40	10 07 37.3	+16 07 46.2	21.25	20.99	20.81	0.44	296.0 ± 3.9	S11
300S-41	10 07 40.2	+15 58 55.6	21.32	20.96	20.80	0.52	295.8 ± 3.8	S11
300S-42	10 07 42.5	+16 00 06.8	22.47	22.02	21.46	1.01	296.6 ±10.3	S11
300S-43	10 07 43.8	+15 49 32.9	22.47	20.98	20.36	2.11	299.2 ± 2.5	S11
300S-44	10 07 47.2	+16 05 45.5	20.13	19.77	19.67	0.46	294.3 ± 2.4	S11
300S-45	10 07 35.9	+16 11 25.7	23.79	22.08	22.00	1.79	242.2 ± 7.8	S11
300S-46	10 06 25.7	+15 54 22.1	21.58	21.13	20.95	0.63	244.3 ± 5.6	S11
300S-47	10 07 11.8	+16 06 30.4	22.80	22.16	21.95	0.85	247.1 ±15.9	S11
300S-48	10 07 07.8	+16 07 21.5	20.64	20.34	20.23	0.41	247.7 ± 2.8	S11
300S-49	10 07 35.2	+15 57 15.3	22.53	21.13	20.41	2.12	255.1 ± 3.0	S11
300S-50	10 06 28.4	+15 56 28.8	17.85	17.56	17.43	0.42	347.1 ± 2.9	S11
300S-51	10 07 36.9	+15 59 58.9	21.99	21.87	21.60	0.39	373.0 ± 6.0	S11
300S-52	10 06 51.7	+16 17 59.2	21.40	20.92	20.95	0.45	394.9 ± 8.9	S11

Note. [a] Target star, referenced as Segue1-11 in N10.

lower confidence in the radial velocity measurement. We also list photometry from the SDSS DR7 (Abazajian et al. 2009).

Figure 1 summarizes the properties of the two samples. The top left panel shows a histogram of the heliocentric radial velocities measured. The central peak (∼270–330 km s^{-1}) has a mean velocity of 300.4 ± 1.1 km s^{-1} and a dispersion of 10.3 ± 1.2 km s^{-1}. Considering the independent N10 and S11 samples separately, we still arrive at a dispersion of 10 km s^{-1} for the central peak, and similar means (303.3 ± 3 km s^{-1} for N10 versus 299.1 ± 1 km s^{-1} for S11). It is not clear whether the intermediate "bridge" candidates with 240 km s^{-1} < $v_{\rm helio}$ < 270 km s^{-1} or the three extreme-velocity stars with $v_{\rm helio}$ > 340 km s^{-1} should be considered part of the same structure, but follow-up observations tracing the stream over a larger field of view could resolve this.

The top right panel of Figure 1 shows the color–magnitude diagram of all the stream candidate stars from Table 1. Here, stream candidates are shown as black circles. (Three stars redder

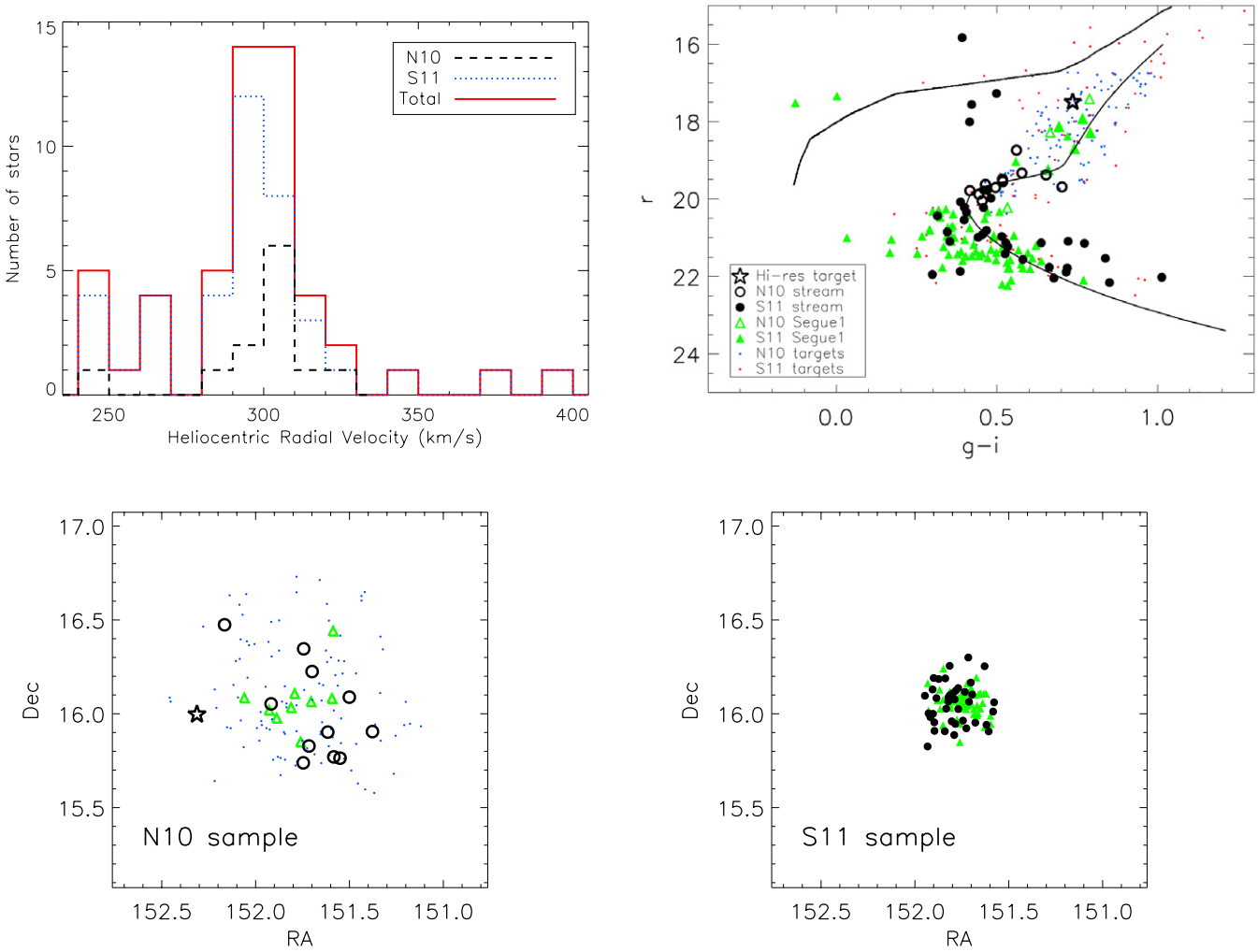

Figure 1. Summarizing the properties of the stream star candidates found in N10 and S11. Top left: heliocentric radial velocity histogram of all stars in the combined N10 and S11 samples with velocities greater than 240 km s^{-1}. The black dashed line shows stars in the N10 sample, the blue dotted lines show stars in the S11 sample, and the solid red line shows the total. Top right: color–magnitude diagram of the 300 km s^{-1} stream candidates found in S11 (filled circles) and N10 (open circles). The open star symbol denotes our target. The green triangles show radial velocity members of the ultra-faint dwarf galaxy Segue 1, among which the stream stars were discovered. Blue (N10) and red (S11) dots show the remaining stars that still meet the photometric cuts in either sample, but are not radial velocity members of Segue 1 or the stream. Photometry is from the SDSS-DR7 (Abazajian et al. 2009). The black line shows the globular cluster sequence of M5 (An et al. 2008), shifted according to reddening ($E(B-V) = 0.03$) and a best-fit distance of 18 kpc. A rough horizontal branch is shown to guide the eye. Bottom: coordinate plots of stream candidate stars, showing the N10 sample (left) and S11 sample (right). The box size represents the 2° field of view covered by N10 centered on Segue 1; S11 on the other hand only observed stars within 15′ of Segue 1's center. Symbols as in the color–magnitude diagram.

(A color version of this figure is available in the online journal.)

than $(g-i) = 1.2$ are not shown.) For comparison, the green triangles show radial velocity members of the Segue 1 dwarf galaxy, which was the target of the N10 and S11 studies. Open symbols show stars from the N10/AAO sample, while filled symbols are from the S11 sample. Note that the N10 sample covers a much larger field of view but does not go as deep—as a result, most of the bright stream stars, including our target (star symbol), show up in this sample. In order to illustrate the photometric criteria used in the samples, the blue and red dots show the stars observed by N10 and S11, respectively, that met their photometric selection cut for follow-up spectroscopy, but are radial velocity non-members of Segue 1 and the stream.

The solid line shows the M5 cluster sequence (An et al. 2008), which gives a good fit to the stream main sequence and subgiant branch when shifted to a distance of 18 kpc. The metallicity of M5 is [Fe/H] = −1.3 (e.g., Carretta et al. 2009), and the SDSS photometry suggests that the 300S is slightly more metal-rich than Segue 1 (Simon et al. 2011). We note, however, that the RGB of the stream is bluer than this sequence, and in principle, would be better fit by the RGB of the more metal-poor globular cluster M92. If done so, the better populated turnoff region is not well fitted, so we adopt the M5 sequence.

There are six stream candidate stars brighter than $r = 19$, and thus possible candidates for high-resolution spectroscopy. Our chosen target (SDSS J100914.95+155948.4; the first star in Table 1) is marked with an open star symbol. It is identified as "Segue 1-11" in N10, but we shall refer to it by "300S-1" throughout this paper. Its location in the color–magnitude diagram indicates that it is most likely a red giant, though it could also be consistent with a horizontal branch star at this distance. Both its colors and the radial velocity of 301 km s^{-1} measured by N10 are consistent with stream membership. A medium-resolution spectrum, taken as part of the N10 campaign, indicates that 300S-1 is more metal-rich than a typical

Table 2
Observed Targets

Name	R.A. (J2000)	Decl. (J2000)	V	$B-V$	UT Date (mm/dd/yyyy)	UT Start	t_{exp} (s)
300S-1	10 09 15.0	+15 59 48.4	17.70[a]	0.68[a]	03/08/2010	02:35	3000
					03/08/2010	05:30	3600
					03/19/2010	05:06	3000
					03/22/2010	00:37	3100
					03/22/2010	05:22	2800
					03/23/2010	05:08	700
HIP37335	07 39 50.1	−01 31 20.4	9.25	0.82	03/13/2011	23:41	7
HIP47139	09 36 20.0	−20 53 14.8	8.34	1.01	03/12/2011	10:08	1
HIP68807	14 05 13.0	−14 51 25.5	7.25	0.93	03/13/2011	23:53	5

Note. [a] Transformed from SDSS photometry following Jordi et al. (2006).

Segue 1 metallicity—consistent with S10's prediction based on isochrone fitting. Accordingly, we deemed it the best candidate for high-resolution spectroscopy follow-up.

The nature of the other five bright stars is less clear. As noted in Geha et al. (2009), random halo stars at these extreme velocities are very rare. If they indeed were turnoff stars, the stream would have a coherent velocity over four magnitudes in distance modulus, which seems unlikely. The three stars around $r \sim 17.5$ could be red horizontal branch stars, but if so, it raises the question of why we do not see more red giants when assuming the numbers of horizontal branch stars and red giants to be roughly equal. The nature of the very bright star at $r = 15.8$ is also not understood but additional data on these brighter stars could provide more insight.

Finally, the spatial coverage of the two samples is shown in the two bottom panels. The brighter stream stars in the N10 sample (left) extend at least over 1° on the sky; the deeper sample of S11 (right) only covers a 15′ radius around the center of Segue 1. The box size here represents the full field of view observed in the N10 sample, and so for the lower left panels, again, all stars observed by N10 are shown to better illustrate the distribution. New photometric observations to determine the full extent of this stream on the sky, as well as deeper observations in a larger region than that covered by S11, would be very important for better understanding and characterizing this structure.

3. OBSERVATIONS AND DATA ANALYSIS

3.1. Observations

We obtained a spectrum of 300S-1 with the MIKE spectrograph (Bernstein et al. 2003) on the Magellan Clay telescope in 2010 March. The total exposure time for this $V = 17.6$ mag star was 4.5 hr, distributed over six exposures to allow for removal of cosmic rays. MIKE spectra have nearly full optical wavelength coverage from ∼3500 to 9000 Å. Using a 1.″0 slit and 2 × 2 on-chip binning, a resolution of ∼22 000 is achieved in the red, and ∼28 000 in the blue wavelength regime.

The data were reduced using an echelle data reduction pipeline made for MIKE.[6] The reduced individual orders were normalized and merged to produce final one-dimensional blue and red spectra ready for the analysis. The signal-to-noise ratio (S/N) of the data of this faint object is modest: 17 at ∼4500 Å and 20 at ∼5200 Å.

In addition to our main target, we also took MIKE spectra of three bright comparison stars chosen from the Fulbright (2000, hereafter F00) sample in 2011 March. These comparison stars were chosen based on having stellar parameters and metallicities that bracketed our first estimate for 300S-1. Table 2 summarizes the observations of our targets. Spectra were taken with a 1.″0 slit and short exposures, in order to get a similar data quality and S/N to that of the 300S-1 spectrum. Figure 2 shows the spectrum of 300S-1 and the short-exposure spectra of the comparison stars in the region around the Mg b lines at 5170 Å. By comparing stellar parameters and abundances derived from these short-exposure spectra to the published values, we are able to assess the accuracy of our low S/N spectrum of 300S-1.

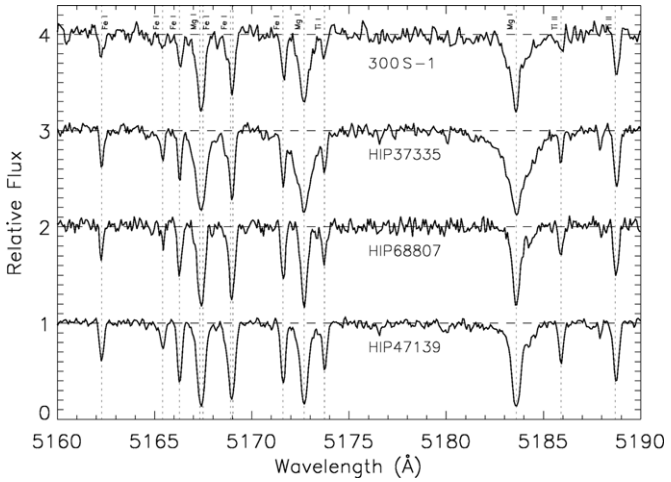

Figure 2. High-resolution spectrum of our target star, 300S-1, and the three comparison stars from the F00 sample, in the region around the Mg b lines. Shown here are the short exposures of the comparison stars, taken to obtain a similar resolution and S/N as the 300S-1 spectrum.

3.2. Line Strength Measurements

We obtained a first estimate for the radial velocity from the two strong Mg b lines in the green region of the spectrum, and two additional Mg lines in the blue. Equivalent widths were then measured by fitting Gaussian profiles to the metal absorption lines, and our estimate was corrected based on the mean radial velocity from all the lines measured. Using these 366 lines, we find a heliocentric radial velocity of 307.6 km s^{-1}, with a standard error of the mean of 0.1 km s^{-1}. This is slightly higher than the estimate of 301 km s^{-1} from N10 based on the medium-resolution spectrum, but consistent within their estimated velocity uncertainty of 10 km s^{-1}. However,

[6] Available at http://obs.carnegiescience.edu/Code/python

Table 3
Derived Stellar Parameters

Name	$T_{\rm eff}$ (K)	log g (dex)	[Fe/H] (dex)	v_t (km s^{-1})
300S-1	5200	2.6	−1.4	1.5
HIP37335[a]	5100 (4850)	2.9 (2.7)	−1.0 (−1.2)	1.5 (1.5)
HIP47139	4550 (4600)	0.9 (1.3)	−1.6 (−1.4)	2.3 (1.8)
HIP68807	4600 (4575)	1.0 (1.1)	−1.8 (−1.8)	2.0 (1.9)

Notes. [a] While our solution for HIP37335 is warmer than what was found in F00, we note that it agrees with other literature sources for this star (e.g., Soubiran et al. 2008; Cenarro et al. 2007; Peterson 1981). The values in parenthesis are those determined by F00, for comparison.

our measurement is well within the estimated range for the 300 km s^{-1} stream.

The line list used for the abundance analysis is based on lines presented in Roederer et al. (2010), Aoki et al. (2007), and Cayrel et al. (2004). In the instances where the same line was included in more than one (original) line list, the most up-to-date oscillator strength was used, following Roederer et al. (2010). This line list was initially compiled for work on stars more metal-poor than the target, but besides the strongest lines, we found it to work well for this metallicity range also.

For atomic lines, equivalent widths were measured by fitting Gaussian profiles. Lines with reduced equivalent widths log(EW/λ) > −4.5 were not used for abundance determination, since they fall near the flat part of the curve of growth. Given the noise in the spectra, most lines with EW $\lesssim$ 20 mÅ, were cautiously excluded from the analysis, except for when the S/N in the respective wavelength range allowed for a $>3\sigma$ detection (e.g., in the red spectral region).

For molecular features and elements with hyperfine splitting, we used a spectrum synthesis approach. The abundance was then determined by matching synthesized spectra of different abundances to the observed spectra (see Section 4 for details).

3.3. Stellar Parameters

The stellar parameters were determined by using the iron lines in each spectrum, by an iterative process. First, the microturbulence is fixed by demanding that the line abundances show no trend with reduced equivalent width (log EW/λ). Similarly, effective temperature is set by requiring no trend of abundance with excitation potential of the lines. Finally, the gravity is fixed by requiring that the abundance derived from Fe II lines agree with that obtained from Fe I to within 0.05 dex. By varying the temperature and microturbulence, and comparing the slope to the scatter in the data, we adopt an uncertainty of ±150 K in temperature, and ±0.3 km s^{-1} in microturbulence. Similarly, we obtain an uncertainty in the gravity of ±0.4 dex by seeing how much the gravity can be changed with Fe I and Fe II still being consistent within their uncertainties.

Table 3 shows the resulting stellar parameters for 300S-1 and the three comparison stars obtained with this method, with the values obtained by F00 in parenthesis for comparison. For HIP68807 and HIP47139, our solutions agree well with the parameters published by F00. For HIP37335, we arrive at a slightly higher temperature and gravity, and thus metallicity, than F00.

Figure 3 shows the adopted stellar parameters overplotted with theoretical 10 Gyr isochrones (Kim et al. 2002). Our values agree reasonably well with the tracks within their uncertainties. As its position on the color–magnitude diagram suggested,

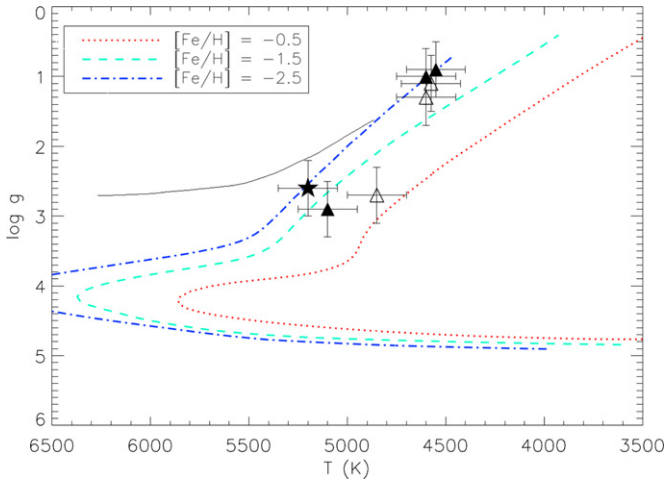

Figure 3. Adopted stellar parameters for 300S-1 (filled star), as well as for the three comparison stars (filled triangles). The open triangles show the values for the comparison stars from Fulbright (2000). Error bars are ±150 K and 0.4 dex in log g. Also shown are theoretical 10 Gyr isochrones at [Fe/H] = −2.5, −1.5, and −0.5, respectively (Kim et al. 2002). A metal-poor horizontal branch has been added to guide the eye.

(A color version of this figure is available in the online journal.)

spectroscopically derived stellar parameters confirm that 300S-1 is located on the RGB. We note that the choice for the age of the isochrone does not influence any conclusion since the giant branches are nearly identical for 10 and, e.g., 12 Gyr.

For comparison, we also use the SDSS colors of 300S-1 to determine the temperature photometrically by interpolating the SDSS *ugriz* colors to the isochrones from Kim et al. (2002), using the color tables of Castelli (http://wwwuser.oat.ts.astro.it/castelli/). This results in a slightly warmer temperature (depending on which colors we use), with $T_{\rm eff} \sim 5400$ K and log $g \sim 3.5$. If we instead use this set of stellar parameters, we would arrive at [Fe/H] of −1.3. This is, however, well within our estimate of uncertainty for the metallicity (see Section 4.4). For the rest of the analysis, we use the parameters derived from spectroscopy to facilitate the relative analysis with the Fulbright (2000) stars.

3.4. Model Atmospheres

Our abundance analysis utilizes one-dimensional plane-parallel Kurucz model atmospheres with overshooting and α-enhancement (Kurucz 1993). They are computed under the assumption of local thermodynamic equilibrium. We use the 2010 version of the MOOG synthesis code (first described in Sneden 1973) for this analysis. In this version, scattering is currently treated as true absorption, which may have consequences for abundances derived from lines in the blue region of the spectrum. Hollek et al. (2011) tested how the stellar parameters are influenced by that effect and found that temperature and gravities, and hence [Fe/H], are somewhat lower (0.1–0.2 dex) when scattering is properly treated. This average abundance difference could be explained by the fact that abundances of metal lines at lower wavelengths (below ∼4200 Å) yield lower abundances when the scattering is treated as Rayleigh scattering. They used metal lines down to 3750 Å. However, [X/Fe] values were found to not change beyond ∼0.05 dex. Similar results were found by Frebel et al. (2010) and Venn et al. (2012). Hence, our star might be a little more metal-poor (perhaps 0.1 dex), because we have no metal lines bluer than 4000 Å and the abundance ratios would not be significantly affected by these different treatments. As discussed below, these effects are well accounted for

Table 4
300S-1 Abundances

Element	$\log\epsilon(X_\odot)$ (dex)	$\log\epsilon(X)$ (dex)	σ (dex)	N	[X/H] (dex)	[X/Fe] (dex)
C (CH)	8.43	7.24	0.21	2	−1.19	+0.27
Na I	6.24	4.93	0.08	3	−1.31	+0.15
Mg I	7.60	6.30	0.07	6	−1.30	+0.16
Al I	6.45	<5.00	···	2	<−1.45	<0.01
Ca I	6.34	5.30	0.06	16	−1.04	+0.42
Sc II	3.15	1.46	0.05	3	−1.69	−0.23
Ti I	4.95	3.69	0.07	18	−1.26	+0.20
Ti II	4.95	3.77	0.06	17	−1.18	+0.28
Cr I	5.64	3.96	0.05	8	−1.68	−0.22
Mn I	5.43	3.41	0.07	3	−2.02	−0.56
Fe I	7.50	6.04	0.05	103	−1.46	0.00
Fe II	7.50	6.08	0.05	10	−1.42	+0.04
Co I	4.99	3.29	0.12	3	−1.70	−0.24
Ni I	6.22	4.73	0.06	14	−1.49	−0.03
Zn I	4.56	3.18	0.25	2	−1.38	+0.08
Sr II	2.87	0.50:	0.40	1	−2.37	−0.91
Ba II	2.18	0.83	0.21	2	−1.35	+0.11
La II	1.10	−0.38	0.30	1	−1.48	−0.02
Eu II	0.52	−0.39:	0.40	1	−0.91	+0.55

in our error budget, and moreover, do not affect our conclusions regarding the nature of 300S-1.

4. ABUNDANCE ANALYSIS OF 300S-1

The derived stellar abundances of 300S-1 are summarized in Table 4. The uncertainties quoted are the standard error of the mean, but we adopt a minimum uncertainty of 0.05 dex. Solar abundances are taken from Asplund et al. (2009). This section discusses the measurement and uncertainties of the different elements in more detail.

4.1. Carbon

The carbon abundance was determined by synthesis of the carbon G-band head at 4313 Å and the CH feature at 4323 Å. An example of this, comparing the observed spectrum to four synthesized spectra, is shown in Figure 4. Here, the thick red line shows the carbon abundance adopted for this region, while the blue and green show the synthesis with Δ[C/Fe] $\pm$ 0.3 dex. Synthesis of the feature at 4323 Å was done independently; the carbon abundance quoted in Table 4 is the mean of the two. Given the noise in the data, we adopt an uncertainty of $\pm$0.3 dex for each measurement.

4.2. Light Elements

Abundances of elements without hyperfine structure were determined from the equivalent width measurements, as described in Section 3.2. In that case, the uncertainties listed in Table 4 are the standard error of the mean of the abundances determined from the individual lines for each element. Abundances of elements with hyperfine structure (Mn and Co) were determined by synthesis of individual lines.

In general, the abundance patterns derived from the high-resolution spectrum are similar to those of outer halo stars at this metallicity (also see Section 5.4 and Figure 7). The possible exception is Mg, which at [Mg/Fe] = 0.14 is low compared to the other α-elements. We note, however, that the derived Mg abundance is very sensitive to the assumed surface gravity in the model, and that our Mg measurements for the three comparison stars are lower than that measured in F00 (also see Section 4.4 and Table 6), so this could be a systematic effect. Taking the α-element abundance as (Ca + Mg + Ti)/3, we find [α/Fe] = +0.26. 300S-1 is at the low end of α-enhancement compared to most halo stars at this metallicity, but still higher than α-abundances seen in classical dwarf spheroidal galaxies (e.g., Tolstoy et al. 2009).

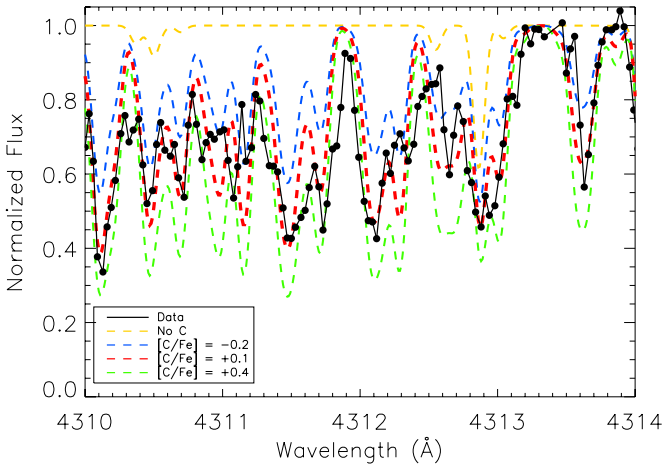

Figure 4. Example of determining carbon abundance by synthesis: the black dotted line shows the actual spectrum of 300S-1 at the carbon G band, while the colored lines show synthesized spectra at different carbon abundances.
(A color version of this figure is available in the online journal.)

4.3. Neutron-capture Elements

Strontium abundance was determined by synthesis of the line at 4215 Å, illustrated in Figure 5. The line at 4077 Å is also visible in the spectrum but too noisy to use for abundance determination; the data are however not inconsistent with what is determined from the line at 4215 Å, within the uncertainties. Given the noise level even at 4215 Å, compared to the difference between the synthesized spectra, this value should be regarded as uncertain. In particular, even though the Sr abundance appears abnormally low compared to other stellar populations in Figure 8, this is likely not significant given the uncertainty.

Barium abundance was determined by synthesis of the lines at 4554 and 6496 Å, with the abundance quoted in Table 4 being the average of the two. The synthesis of the 6496 Å line is shown in Figure 5. We adopt an uncertainty of $\pm$0.3 dex. Europium was determined by synthesis of the line at 4129 Å. Like strontium, there is considerable uncertainty due to the noisy spectrum. Lanthanum was determined by synthesis of the line at 4333 Å. Other lines are visible but too noisy for more precise abundance determination; the upper limits derived are however consistent with the result derived from the line at 4333 Å. Synthesis of the 4333 Å line is shown in Figure 5.

4.4. Uncertainties

Random errors come from uncertainties in placing the continuum level; we estimate the random uncertainty in the abundance of an element as the standard error of the mean abundance determined from individual lines. For elements that were determined from fitting just one line with a synthetic spectrum (Sr, Eu, and La), the error quoted in the second column is the estimated fitting uncertainty.

Systematic errors arise from uncertainties in the stellar parameters, as described in Section 3.3. To quantify this effect, we repeated the analysis with the stellar parameters of 300S-1

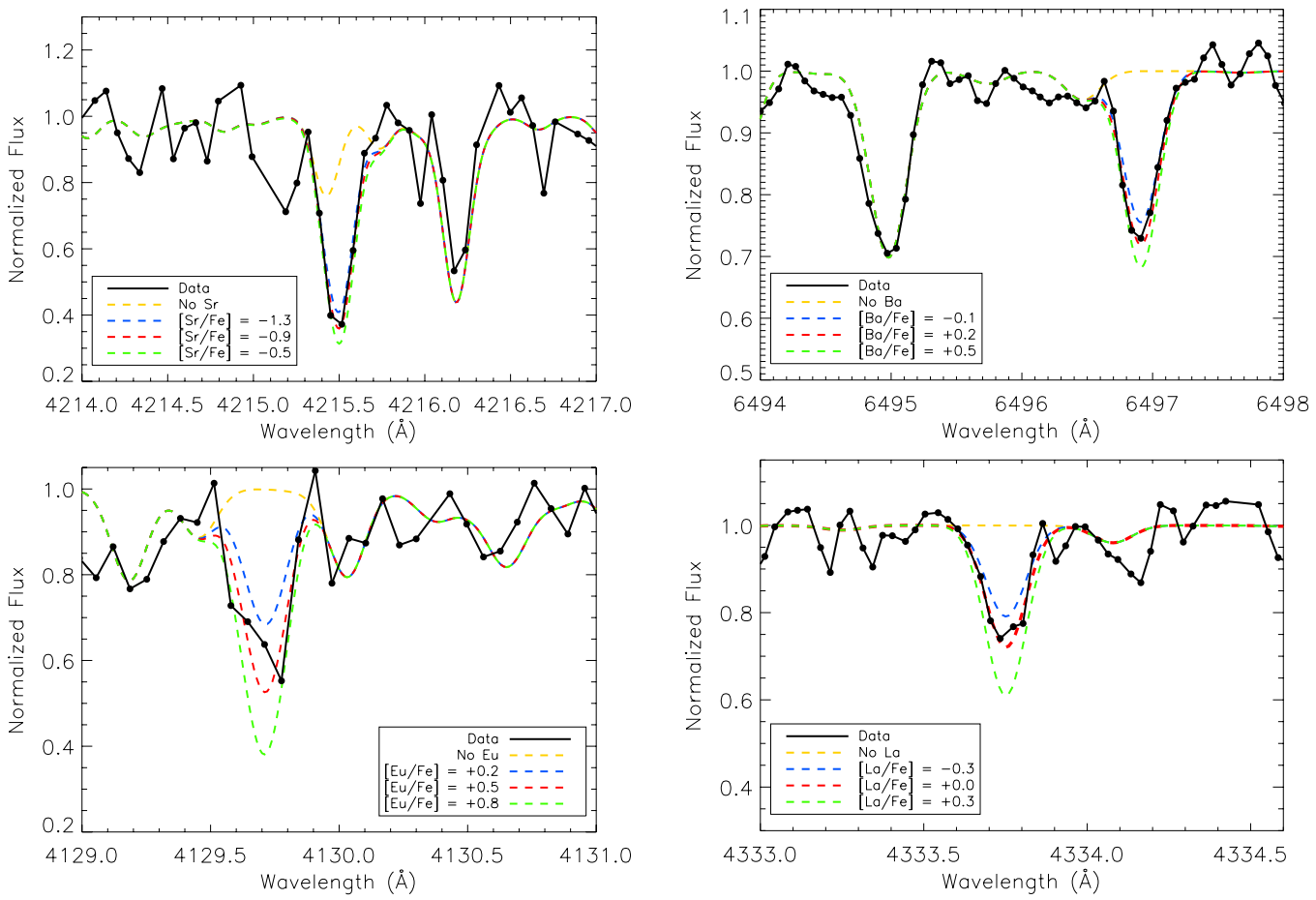

Figure 5. Determining the abundances of Sr, Ba, Eu, and La by comparing the observed lines to synthesized spectra at different abundances.
(A color version of this figure is available in the online journal.)

Table 5
Abundance Uncertainties for 300S-1

Elem.	Random Uncer.	$\Delta T_{\rm eff}$ +150 K	$\Delta \log g$ +0.4 dex	$\Delta v_{\rm micr}$ +0.3 km s^{-1}	Total Uncer.
C (CH)	0.21	0.30	−0.05	−0.02	0.37
Na I	0.08	0.16	−0.10	−0.04	0.21
Mg I	0.07	0.16	−0.11	−0.05	0.21
Ca I	0.06	0.13	−0.05	−0.10	0.18
Sc II	0.05	0.02	+0.16	−0.02	0.17
Ti I	0.07	0.20	−0.02	−0.09	0.23
Ti II	0.06	0.03	+0.15	−0.09	0.19
Cr I	0.05	0.19	−0.01	−0.08	0.21
Mn I	0.07	0.15	−0.03	−0.10	0.20
Fe I	0.05	0.18	−0.04	−0.13	0.23
Fe II	0.05	−0.02	+0.16	−0.09	0.19
Co I	0.12	0.25	+0.00	−0.20	0.34
Ni I	0.06	0.14	+0.00	−0.06	0.16
Zn I	0.25	0.04	+0.10	−0.05	0.28
Sr II	0.40	0.10	+0.02	−0.10	0.42
Ba II	0.21	0.09	+0.08	−0.18	0.30
La II	0.30	0.05	+0.15	−0.05	0.34
Eu II	0.40	0.05	+0.15	−0.05	0.43

changed by +150 K, +0.4 dex, and +0.3 km s^{-1} in temperature, log g and microturbulence, respectively, and record the corresponding change in abundance. Table 5 shows the result. The total uncertainty is obtained by summing the individual components in quadrature.

Another assessment of the uncertainties, given the modest data quality, comes from comparing our abundances from the low S/N spectra of the comparison stars with those of F00. Table 6 shows the derived abundances of the comparison stars, and lists the published values from F00 also. Our abundances are in good agreement within the uncertainties, especially when taking into account the different stellar parameter solution for HIP37335.

5. CHARACTERIZING THE 300 km s^{-1} STREAM

5.1. Stream Membership

As demonstrated by other authors, there is unequivocally a coherent stream present here with a kinematic peak at $v_{\rm helio} = 300$ km s^{-1} (Geha et al. 2009; Norris et al. 2010; Simon et al. 2011). With more extreme velocities, halo contaminants become less likely. Given that a stream is present here with high velocities, it is worth quantifying the probability whether the star analyzed here is a background halo star or not. We have employed a two-sample Kolmogorov–Smirnov test using the predicted line-of-sight velocities from the Besançon model (Robin et al. 2003) to quantify this likelihood. We find a p value of 0.097, or a ∼10% chance that 300S-1 and predicted stars in the Besançon model (Robin et al. 2003) are drawn from the same distribution. It is clear that this star sits separate from the main line-of-sight predicted population (Figure 6).

We can also deduce some likelihood that 300S-1 is a halo member when we examine the observed velocity distribution in

Table 6
Standard Star Abundances

Element	$\log\epsilon(X)$ (dex)	σ (dex)	N	[X/H] (dex)	[X/Fe] (dex)	$[X/Fe]_{F00}$ (dex)
			HIP37335			
C (CH)	7.71	0.21	2	−0.72	+0.28	···
Na I	5.46	0.07	4	−0.78	+0.22	+0.32
Mg I	7.05	0.12	4	−0.55	+0.45	+0.63
Ca I	5.86	0.05	16	−0.48	+0.52	+0.44
Sc II	2.40	0.05	9	−0.75	+0.25	···
Ti I	4.20	0.05	28	−0.75	+0.25	+0.26
Ti II	4.20	0.05	16	−0.75	+0.25	···
Cr I	4.65	0.05	14	−0.99	+0.01	−0.05
Mn I	4.61	0.05	3	−0.82	+0.18	···
Fe I	6.50	0.05	124	−1.00	0.00	(−1.26)
Fe II	6.48	0.05	15	−1.02	−0.02	···
Co I	3.55	0.05	3	−1.44	−0.44	···
Ni I	5.30	0.05	24	−0.92	+0.08	+0.10
Zn I	3.78	0.08	2	−0.78	+0.22	···
Ba II	1.43	0.21	2	−0.75	+0.25	−0.02
La II	0.42	0.30	1	−0.68	+0.32	···
Eu II	−0.19	0.30	1	−0.71	+0.29	+0.38
			HIP68807			
C (CH)	6.76	0.21	2	−1.67	+0.19	···
Na I	4.36	0.05	3	−1.88	−0.02	−0.13
Mg I	6.17	0.05	6	−1.43	+0.43	+0.49
Ca I	4.89	0.05	17	−1.45	+0.41	+0.37
Sc II	1.45	0.06	6	−1.70	+0.16	···
Ti I	3.25	0.05	23	−1.70	+0.16	+0.20
Ti II	3.45	0.05	18	−1.50	+0.36	···
Cr I	3.61	0.05	14	−2.03	−0.17	−0.12
Mn I	3.40	0.07	3	−2.03	−0.17	···
Fe I	5.64	0.05	127	−1.86	0.00	(−1.83)
Fe II	5.68	0.05	14	−1.82	0.04	···
Ni I	4.48	0.05	12	−1.74	+0.12	−0.03
Zn I	2.84	0.20	1	−1.72	+0.14	···
Ba II	0.69	0.14	3	−1.49	+0.37	+0.27
La II	−0.68	0.30	1	−1.78	+0.08	···
Eu II	−0.99	0.40	1	−1.51	+0.35	+0.40
			HIP47139			
C (CH)	6.61	0.21	2	−1.82	−0.23	···
O I	8.14	0.15	1	−0.55	+1.04	···
Na I	4.65	0.05	4	−1.59	0.00	−0.18
Mg I	6.42	0.08	4	−1.18	+0.41	+0.54
Ca I	5.05	0.05	16	−1.29	+0.30	+0.27
Sc II	1.64	0.05	12	−1.51	+0.08	···
Ti I	3.52	0.05	26	−1.43	+0.16	+0.29
Ti II	3.67	0.05	18	−1.28	+0.31	···
Cr I	3.94	0.07	16	−1.70	−0.11	−0.17
Mn I	3.58	0.07	3	−1.85	−0.26	···
Fe I	5.91	0.05	109	−1.59	0.00	(−1.46)
Fe II	5.94	0.05	11	−1.56	0.03	···
Ni I	4.65	0.05	18	−1.57	+0.02	+0.00
Zn I	2.97	0.11	2	−1.59	−0.00	···
Ba II	0.92	0.10	3	−1.26	+0.33	+0.16
La II	−0.48	0.30	1	−1.58	+0.01	···
Eu II	−0.49	0.40	1	−1.01	+0.58	···

Figure 1. The peak of the stream velocity distribution occurs at 300 km s^{-1} and comprises 39 member stars, amongst background halo outliers with velocities between 250 and 400 km s^{-1}. Within the 270–330 km s^{-1} range, it is reasonable to suspect that we would observe fewer than 10 halo contaminants in 2° with such high velocities. Indeed, the observed background range in Figure 1 is approximately 5–10 halo stars, suggesting a probability of between 13% and 26% that 300S-1 is a halo contaminant. We note that the probability that this star is a halo star ($\gtrsim$10%) is the same probability cutoff employed by Simon et al. (2011) in examining stream members.

It is well known that RGB stars in globular clusters exhibit a characteristic anti-correlation in Na–O and Al–Mg (Carretta et al. 2009). Due to the low spatial distribution and relatively high kinematic dispersion for this stream compared to typical kinematically cold stellar streams, it is possible that the origin of the 300 km s^{-1} stream is a disrupted globular cluster. Although our spectrum has extremely modest S/N below 4000 Å, we have attempted to synthesize the Al lines at 3944 Å and 3961 Å. The Al lines at ∼6697 Å were not detected. Hence, we cannot determine an accurate value for [Al/Fe] from the blue lines. We can only exclude a super-solar abundance [Al/Fe] < 0 for this star. However, this is a rather low [Al/Fe] abundance if 300S-1 was a member of a globular cluster. While there are globular cluster stars with [Al/Fe] < 0 and similar metallicities, they generally have Mg abundances of $0.3 <$ [Mg/Fe] < 0.6 (compare to Carretta et al. 2009, their Figure 5). 300S-1 has [Mg/Fe] $= 0.14$ and even if that Mg abundance were systematically low by 0.1–0.2 dex, it would still mostly fall outside any covered region. It suggests that 300S-1 may not be of a globular cluster origin. Unfortunately, given the modest S/N of our spectra no reliable upper limit on oxygen could be ascertained that could provide further clues on the topic.

5.2. Metallicity of Stream

We determine a metallicity of [Fe/H] $= -1.46 \pm 0.05 \pm 0.23$ (random and systematic uncertainties) for 300S-1 based on the high-resolution spectrum. This is in agreement with the prediction of [Fe/H] $= -1.3$ from Simon et al. (2011). This is also consistent with what we roughly estimate from fitting the M5 (with [Fe/H] $= -1.2$) isochrone to the stream photometry. It adds support to the result that the stream stars have higher metallicity than the Segue 1 system, as already noted in S11 based on Ca triplet equivalent widths. The AAOmega sample of N10 contains some metallicity estimates based on Ca II K line strengths; in addition to 300S-1, the spectrum of the stream star Segue1-101 (SDSS J100659.01+154418.8) has enough counts to yield [Fe/H] $\simeq -1.7$. Beyond this, there are no additional data to determine the metallicity spread of the stream.

5.3. Evolutionary Status

From the spectroscopic analysis, we find 300S-1 to be an RGB star. Although the star sits slightly above the isochrone, it agrees with the isochrone within the uncertainties in the stellar parameters. From photometry, the star is also found to sit slightly above a shifted M5 globular cluster sequence. It is noteworthy, though, that the scatter of stream members is significant (see Figure 1). Nevertheless, these discrepancies could indicate the star to be on the horizontal branch. The carbon abundance of 300S-1 may shed light on this question. As a star ascends the giant branch, CN cycling converts carbon into nitrogen, thus lowering the observed surface carbon abundances. The measured value of [C/Fe] $= 0.25$ suggests that CN cycling has not yet significantly operated, assuming that the star did not form from an unusually carbon-rich gas cloud. Some globular clusters show this effect (e.g., Carretta et al. 2005, their Figure 7) and compared to that, the carbon abundance of 300S-1 also suggests the star to be on the lower or middle part of the RGB and not in a more evolved state on the horizontal branch.

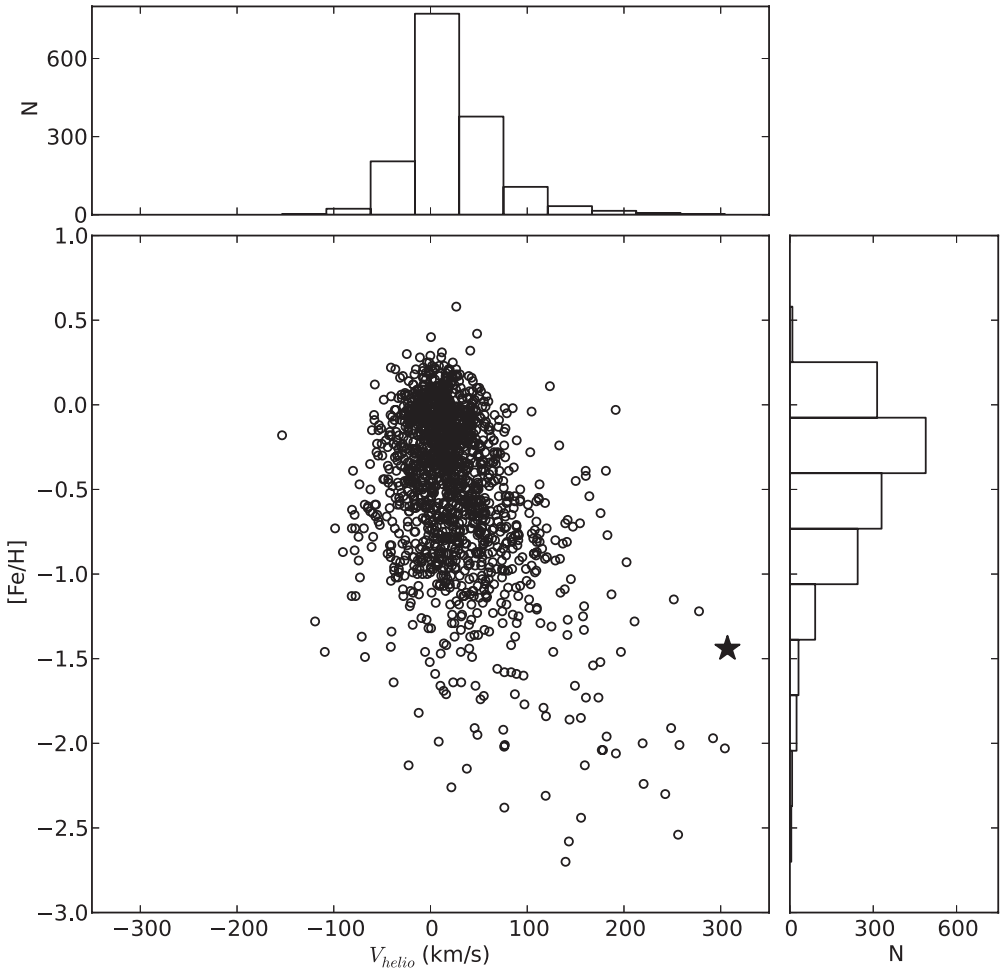

Figure 6. Kinematics and metallicities for line-of-sight stars predicted by the Besançon model (Robin et al. 2003). The star analyzed here, 300S-1, is marked as a filled star.

5.4. Abundance Ratios

Figures 7 and 8 show the abundance patterns of 300S-1, based on our high-resolution spectrum. The blue, cyan, and red points show stars in the halo, thick disk, and thin disk, respectively, from the sample of Fulbright (2000, 2002). Since the Fulbright sample does not include Cr, Sr, and La measurements, comparison points (halo stars) for these elements are taken from Lai et al. (2007) and Barklem et al. (2005). In addition, the crosses show abundance patterns of stars in the classical dwarf galaxies Draco, Sextans, Ursa Minor, Carina, Fornax, Sculptor, and Leo I (Shetrone et al. 2001, 2003; Geisler et al. 2005; Aoki et al. 2009; Cohen & Huang 2009).

The abundance ratios of 300S-1 overlap well with the general halo population at that metallicity, though as noted in Section 4, the α- and particularly Mg abundances are on the low end. (The Sr abundance also appears low, but as discussed in Section 4, this is likely not significant due to the low S/N of the spectrum in this region.) The general abundance pattern is closer to a typical halo star than to a classical dwarf spheroidal galaxy star.

The overall abundance pattern is important for interpreting the nature of the stream and its potential progenitor. Judging from this one star, 300S may be the first stream with halo-like abundances. This predicament illustrates that a careful mapping of the region around Segue 1 and the 300 km s^{-1} stream is of great importance. Initial work on SDSS data to address this question hints that this region is even more complex than assumed thus far. An attempt to decompose the many populations in the Segue 1 region will be presented in a forthcoming paper (A. Jayaraman et al., in preparation).

5.5. Distance to Stream

We use two different methods of estimating the distance to the stream. First, based on the stellar parameters we assume 300S-1 to be a red giant (Figure 3). Given the star's metallicity, we chose the [Fe/H] $= -1.5$ isochrone as the "best fit." While it is not a perfect match to our stellar parameters, it is reasonably close to our determined values. The corresponding inferred absolute magnitude of 300S-1 is $M_V \simeq +1.37$. Transforming the Sloan photometry following Jordi et al. (2006), and correcting for extinction according to Schlegel et al. (1998), we find 300S-1 has $V = 17.60$. This yields a distance modulus of 16.23, resulting in a best distance estimate of $\simeq$18 kpc. Given the uncertainties, however, a distance within $\pm$7 kpc of this estimate would still be consistent with the stellar parameters we derived from the spectroscopy. Our distance estimate of 18 kpc is in good agreement with Simon et al. (2011) who find a distance of 22 kpc to the stream.

A second distance estimate comes from using the photometric data and comparing the color–magnitude diagram to various globular cluster sequences from An et al. (2008), shifted according to the distance moduli and reddening ($E(B - V) = 0.03$

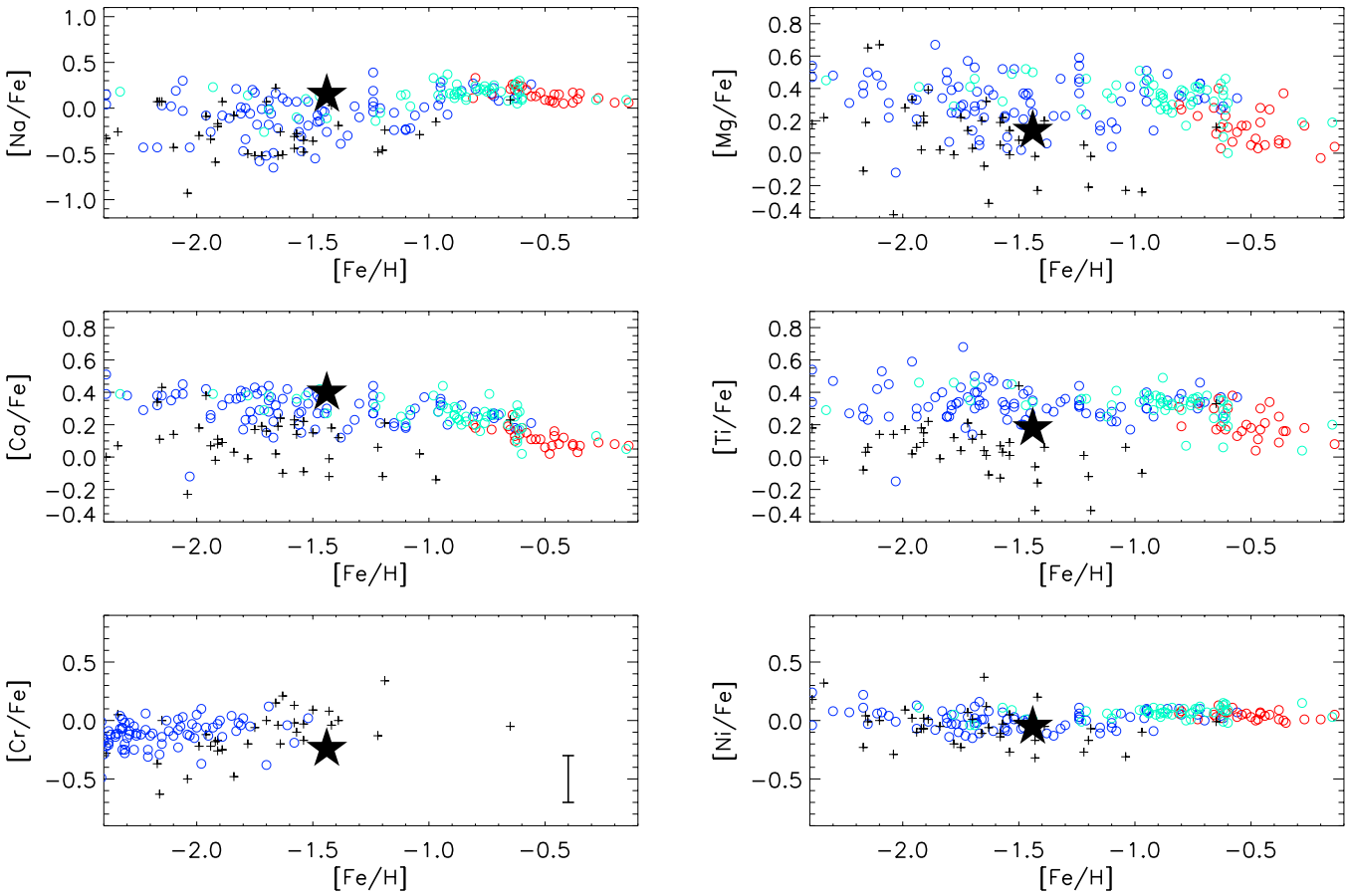

Figure 7. Abundance ratios for light elements in 300S-1 (filled star symbol), as measured from our high-resolution spectrum. For comparison, red and cyan points show thin and thick disk stars, respectively, blue points show halo stars, and the crosses show stars in the classical dwarf galaxies Draco, Sextans, Ursa Minor, Carina, Fornax, Sculptor, and Leo I. A typical error bar for our measurements is shown in the lower left panel (also see Table 5).

(A color version of this figure is available in the online journal.)

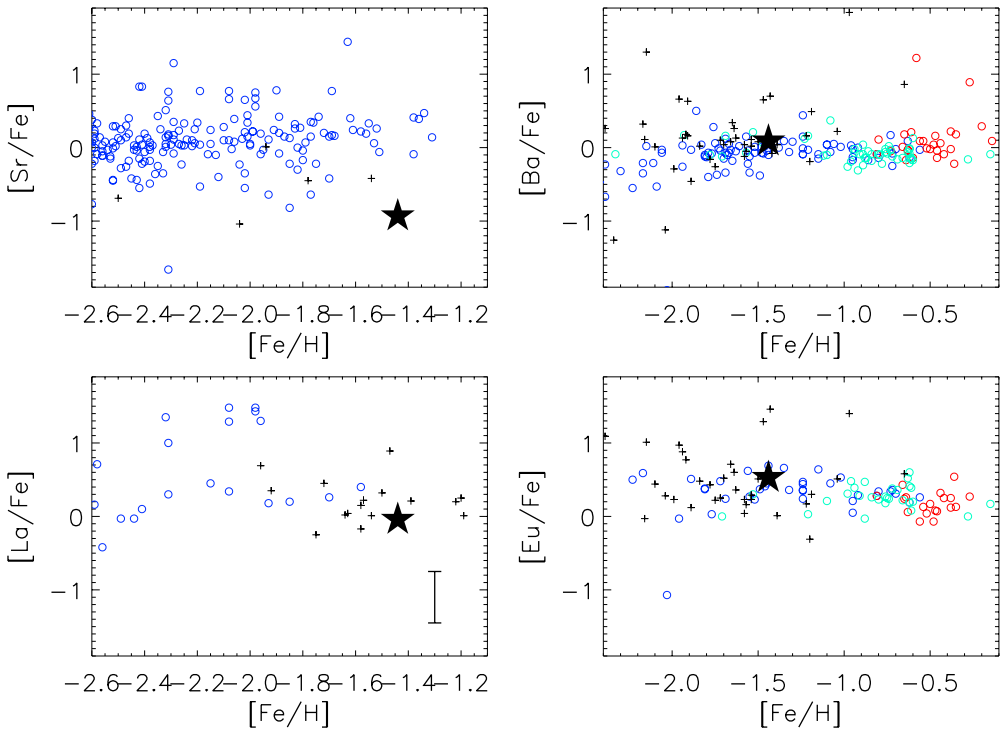

Figure 8. Abundance ratios for the neutron-capture elements Sr, Ba, La, and Eu in 300S-1. Symbols are the same as in Figure 7.

(A color version of this figure is available in the online journal.)

for M5, $E(B-V) = 0.02$ for M92) compiled in Harris (1996). As seen in Figure 1, the M5 sequence is a good fit to the stream data when shifted to a distance of 18 kpc. This is in good agreement with the estimate based on spectroscopically determined stellar parameters.

Both the isochrone fit based on the single spectroscopic measurement and the photometric data indicate that the stream stars are at a distance of $\simeq$18 kpc, slightly closer than the assumed distance of 23 ± 2 kpc (Belokurov et al. 2007b) for Segue 1 itself. However, the uncertainties on both values are substantial enough that we cannot rule out that they are at the same distance. We also caution that since the stream stars were picked out in color–magnitude filters targeting stars at the distance of Segue 1, the stream stars in our sample by design cannot be at a very different distance.

We note that with galactic coordinates $l, b \simeq 220^\circ, 50^\circ$ and a heliocentric distance of 18 kpc, the stream stars are located in the outer galaxy. A heliocentric radial velocity of 300 km s^{-1} translates to a Galactic standard of rest velocity of about 230 km s^{-1} in this direction. This suggests the stream stars to be on a low angular momentum orbit that would eventually bring it closer and into the inner Galaxy.

6. CONCLUSIONS

We have presented a high-resolution spectrum and abundance analysis of 300S-1, a bright star in the 300 km s^{-1} stream near the ultra-faint dwarf galaxy Segue 1. We determine a metallicity [Fe/H] $= -1.46 \pm 0.05 \pm 0.23$ (random and systematic uncertainties) for this star, with abundance ratios similar to typical halo stars at this metallicity. Fitting the stellar parameter solution onto theoretical isochrones, we estimate a distance of 18 ± 7 kpc. Both the metallicity and distance are in good agreement with estimates obtained from comparing the SDSS photometry to globular cluster sequences.

With this new information, we present several possible scenarios regarding the nature and origin of the stream.

1. Since these high-velocity stars were discovered in a survey targeting Segue 1 members, a natural question to ask is whether the stream is related to the Segue 1 dwarf galaxy. We find this an unlikely scenario for several reasons. First, the study of S11 finds no evidence that the Segue 1 system is being tidally disrupted. Our distance estimate, based both on the high-resolution spectroscopy data and the photometry, indicates that the stream stars are at a slightly closer distance than Segue 1, though the data are not good enough to rule out that they are at the same distance. In addition, the color–magnitude diagrams suggest that the stream members are in general at a higher metallicity than Segue 1, which our high-resolution measurement of one stream star also confirms.
2. Another possibility, suggested by Geha et al. (2009), is that these stars could be associated with the Sagittarius Stream. Indeed at least two wraps of Sagittarius overlap with Segue 1 in this direction, and Niederste-Ostholt et al. (2009) argue that Segue 1 itself is a star cluster from the Sagittarius galaxy. But as for the stream stars, our metallicity measurement indicates that the 300 km s^{-1} stream does not have metallicities representative of Sgr debris (Chou et al. 2007; Casey et al. 2012), and no Sgr debris model that we are aware of predicts a wrap at this velocity. Moreover, the part of the Sagittarius Stream proposed to be contaminating Segue 1 samples has $v_{\rm GSR} \sim 130$ km s^{-1} (Niederste-Ostholt et al. 2009), while the stream stars have $v_{\rm GSR} \sim 230$ km s^{-1}.
3. The Orphan Stream (Belokurov et al. 2007a) crosses the Sagittarius Stream on the sky near Segue 1, and at a similar distance modulus. Again, however, the velocities do not agree—the reported velocities of the Orphan Stream are around $v_{\rm GSR} \sim 110$ km s^{-1}. In addition, the Orphan Stream is metal-poor, with reported metallicities of [Fe/H] $= -1.63$ to -2.10 (Newberg et al. 2010; Casey et al. 2013). Although both the Orphan Stream and Sagittarius Stream overlap with the 300 km s^{-1} stars, the combined metallicity and velocity information suggests that they are unrelated.
4. Carlin et al. (2012) suggest that the stream is debris associated with the Virgo substructure, based on kinematics and metallicities. However, we have assumed throughout this paper that the 300 km s^{-1} feature is a stellar stream, but as pointed out in S11, until we can determine the full spatial extent of these kinematically linked stars, we cannot rule out that the stars belong to a bound object. If so, given the 1° extent seen in N10, its physical diameter would be at least 300 (d/18 kpc) pc. This highlights the need for new photometry to map out the full extent of the 300 km s^{-1} stars.

The fact that this stream may be largely chemically similar to the halo is particularly interesting. This is relevant to chemical tagging (Freeman & Bland-Hawthorn 2002), which infers that stars originating from a common origin can be unambiguously identified solely by their chemistry and without the need for kinematics. This stream is most noticeable only from its kinematics, and not by any particularly distinct chemical signature identified in this work. Although the luminosity, number of abundances analyzed or abundance uncertainties presented here do not match the strict requirements for the complete chemical tagging planned in future galactic archaeology surveys (Ting et al. 2012), we identify this 300 km s^{-1} stream as a candidate for testing and validating the chemical tagging concept. It would be particularly interesting to determine whether chemical tagging alone could identify members belonging to this 300 km s^{-1} stream without the need for kinematics, as the chemical elements analyzed here are only marginally distinguishable from the halo.

Although the 300 km s^{-1} stars are found in a region of sky with many known structures, the combination of velocity, chemistry, and distance information makes it unlikely that these stars are associated with any of the Sagittarius Stream, the Orphan Stream, or the Segue 1 dwarf galaxy. We therefore conclude that these stars belong to a new structure in the crowded "Field of Streams." Its features include an extreme mean velocity of 300 km s^{-1} with a velocity dispersion of 7 km s^{-1} (as found by S11), a broad spatial distribution, and halo-like chemical abundances. The abundance patterns in particular make this stream very interesting to study in the context of halo formation.

A.F. acknowledges support of an earlier Clay Fellowship administered by the Smithsonian Astrophysical Observatory. A.R.C. acknowledges the financial support through the Australian Research Council Laureate Fellowship 0992131, and from the Australian Prime Minister's Endeavour Award Research Fellowship, which has facilitated his research at MIT. J.E.N. acknowledges support from the Australian Research Council (grants DP063563 and DP0984924) for studies of the Galaxy's most metal-poor stars and ultra-faint satellite systems.

R.F.G.W. acknowledges support from NSF grants AST-0908326 and CDI-1124403.

Facility: Magellan:Clay (MIKE)

REFERENCES

Abazajian, K. N., Adelman-McCarthy, J. K., Agüeros, M. A., et al. 2009, ApJS, 182, 543
An, D., Johnson, J. A., Clem, J. L., et al. 2008, ApJS, 179, 326
Aoki, W., Arimoto, N., Sadakane, T., et al. 2009, A&A, 502, 569
Aoki, W., Honda, S., Beers, T. C., et al. 2007, ApJ, 660, 747
Asplund, M., Grevesse, N., Sauval, A. J., & Scott, P. 2009, ARA&A, 47, 481
Barklem, P. S., Christlieb, N., Beers, T. C., et al. 2005, A&A, 439, 129
Belokurov, V., Evans, N. W., & Irwin, M. 2007a, ApJ, 658, 337
Belokurov, V., Zucker, D. B., Evans, N. W., et al. 2006, ApJL, 642, L137
Belokurov, V., Zucker, D. B., & Evans, N. W. 2007b, ApJ, 654, 897
Bernstein, R., Shectman, S. A., Gunnels, S. M., Mochnacki, S., & Athey, A. E. 2003, Proc. SPIE, 4841, 1694
Carlin, J. L., Yam, W., Casetti-Dinescu, D. I., et al. 2012, ApJ, 753, 145
Carretta, E., Bragaglia, A., Gratton, R. G., & Lucatello, S. 2009, A&A, 505, 139
Carretta, E., Gratton, R. G., Lucatello, S., Bragaglia, A., & Bonifacio, P. 2005, A&A, 433, 597
Casey, A. R., Da Costa, G., Keller, S. C., & Maunder, E. 2013, ApJ, 764, 39
Casey, A. R., Keller, S., & Da Costa, G. 2012, AJ, 143, 88
Cayrel, R., Depagne, E., Spite, M., et al. 2004, A&A, 416, 1117
Cenarro, A. J., Peletier, R. F., Sánchez-Blázquez, P., et al. 2007, MNRAS, 374, 664
Chou, M.-Y., Majewski, S. R., Cunha, K., et al. 2007, ApJ, 670, 346
Cohen, J. G., & Huang, W. 2009, ApJ, 701, 1053
Frebel, A., Simon, J. D., Geha, M., & Willman, B. 2010, ApJ, 708, 560
Freeman, K., & Bland-Hawthorn, J. 2002, ARA&A, 40, 487
Fulbright, J. P. 2000, AJ, 120, 1841
Fulbright, J. P. 2002, AJ, 123, 404
Geha, M., Willman, B., Simon, J. D., et al. 2009, ApJ, 692, 1464
Geisler, D., Smith, V. V., Wallerstein, G., Gonzalez, G., & Charbonnel, C. 2005, AJ, 129, 1428
Harris, W. E. 1996, AJ, 112, 1487
Hollek, J. K., Frebel, A., Roederer, I. U., et al. 2011, ApJ, 742, 54
Ibata, R. A., Gilmore, G., & Irwin, M. J. 1994, Natur, 370, 194
Jordi, K., Grebel, E. K., & Ammon, K. 2006, A&A, 460, 339
Kim, Y.-C., Demarque, P., Yi, S. K., & Alexander, D. R. 2002, ApJS, 143, 499
Kurucz, R. L. 1993, Kurucz CD-ROM 13, ATLAS9 Stellar Atmosphere Programs and 2 km/s Grid (Cambridge, MA: SAO)
Lai, D. K., Johnson, J. A., Bolte, M., & Lucatello, S. 2007, ApJ, 667, 1185
Lynden-Bell, D., & Lynden-Bell, R. M. 1995, MNRAS, 275, 429
Majewski, S. R., Skrutskie, M. F., Weinberg, M. D., & Ostheimer, J. C. 2003, ApJ, 599, 1082
Newberg, H. J., Willett, B. A., Yanny, B., & Xu, Y. 2010, ApJ, 711, 32
Niederste-Ostholt, M., Belokurov, V., Evans, N. W., et al. 2009, MNRAS, 398, 1771
Norris, J. E., Wyse, R. F. G., Gilmore, G., et al. 2010, ApJ, 723, 1632
Peterson, R. C. 1981, ApJ, 244, 989
Robin, A. C., Reylé, C., Derrière, S., & Picaud, S. 2003, A&A, 409, 523
Roederer, I. U., Sneden, C., Thompson, I. B., Preston, G. W., & Shectman, S. A. 2010, ApJ, 711, 573
Schlegel, D. J., Finkbeiner, D. P., & Davis, M. 1998, ApJ, 500, 525
Shetrone, M., Venn, K. A., Tolstoy, E., et al. 2003, AJ, 125, 684
Shetrone, M. D., Côté, P., & Sargent, W. L. W. 2001, ApJ, 548, 592
Simon, J. D., Geha, M., Minor, Q. E., et al. 2011, ApJ, 733, 46
Sneden, C. A. 1973, PhD thesis, Univ. Texas, Austin
Soubiran, C., Bienaymé, O., Mishenina, T. V., & Kovtyukh, V. V. 2008, A&A, 480, 91
Ting, Y. S., Freeman, K. C., Kobayashi, C., de Silva, G. M., & Bland-Hawthorn, J. 2012, MNRAS, 421, 1231
Tolstoy, E., Hill, V., & Tosi, M. 2009, ARA&A, 47, 371
Venn, K. A., Shetrone, M. D., Irwin, M. J., et al. 2012, ApJ, 751, 102